Pitting Corrosion Resistance of a 316L Stainless Steel Manufactured by the Direct Metal Laser Sintering Process

C. Prieto, D. Young, M. Singer
Institute for Corrosion and Multiphase Technology
Department of Chemical and Biomolecular Engineering
Ohio University
Athens, OH 45701

M. Clum, T. J. Cyders
Department of Mechanical Engineering
Ohio University
Athens, OH 45701

ABSTRACT

Direct metal laser sintering (DMLS) is an additive manufacturing process that utilizes a laser to sinter powdered metal to make geometrically complex parts. However, DMLS generally produces material with lower mechanical performance and higher anisotropy as compared to conventional manufacturing approaches of the same material. Furthermore, components made by DMLS are believed to be more vulnerable to corrosion due to the presence of residual porosity, as well as laser induced microstructural deformations. This research focuses on the evaluation of the pitting corrosion resistance of 316L stainless steel manufactured using DMLS. Rolled 316L stainless steel specimens with similar chemical composition were used as a reference to compare their microstructural characteristics, porosity and pitting corrosion resistance. The microstructure of the DMLS samples was also compared to specimens annealed to eliminate laser induced scan tracks. Porosity of the DMLS specimens were determined per ASTM B311. Profilometry, compositional analysis and quantification of the corrosion resistance were performed, before and after the corrosion pitting resistance test, per ASTM G48 Method A (ferric chloride pitting test).

Key words: 316L stainless steel, ASTM G48, ASTM G5, ASTM B311, DMLS, pitting corrosion

INTRODUCTION

Additive manufacturing using selective laser melting is a relatively new and advanced process for making geometrically elaborated metallic parts, utilizing output from computer-aided design (CAD) programs[1,2]. Each variant of this manufacturing process has, at its heart, a layer-by-layer forming approach; each layer is *ca.* 20 μm in thickness. The layers are composed of powdered metal sintered using powder bed fusion (PBF) methods, such as by direct metal laser sintering (DMLS)[1,3]. The DMLS technique uses a laser to increase the temperature of the metal powder and induce sintering[1,4]. An illustration of this process is shown in Figure 1.
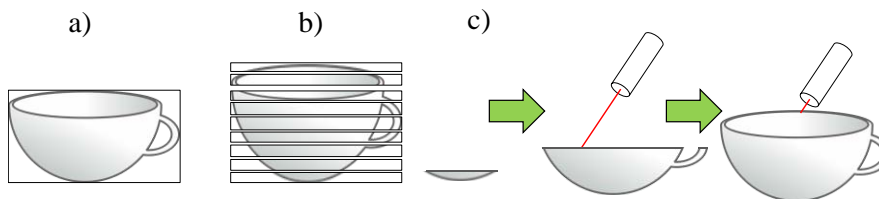
Figure 1. Schematic for the direct metal laser sintering additive manufacturing process: a) Generate a CAD file for an object; b) the object is divided into horizontal layers; c) the machine reads the CAD file for the layered object and sinters metal powder layer-by-layer (of the order of 20µm for each layer) until the product is finished. Adapted from Gibson, *et al.*[1]

The DMLS process has significant advantages for production, such as reducing the amount of base material required to produce a piece, decrease the time of manufacturing, and increase precision relating to part formation.[1–3] However, these advantages can potentially be lost if the mechanical properties and corrosion resistance of the final product are compromised. Porosity, scan tracks and an inhomogeneous microstructure can be present in the final product,[1–5] since the manufacturing process involves the coalescence of the metal powder by heating and rapid cooling.[1,3] One solution to overcome the aforementioned drawbacks from the DMLS process is the selection of materials with excellent corrosion resistance properties, such as austenitic stainless steels.[1,6] Among the austenitic stainless steels, series 300 alloys with low carbon content are widely used in this type of manufacturing process.[1,3,6–8] Within the 300 series of austenitic stainless steel, the 316L stainless steel (L implies low carbon content) is one of the materials that can be potentially used for harsher environments; it includes molybdenum (Mo) which increases the pitting resistance to chlorides in acidic environments.[9] The resistance to corrosion and preservation of mechanical properties are crucial factors for potential application of products manufactured from DMLS 316L stainless steel. Consequently, the current research is focused on assessing the pitting corrosion resistance of a 316L stainless steel made by DMLS.

Corrosion of Austenitic Stainless Steels

Corrosion of austenitic steel can be classified as general and localized[10]. General corrosion of austenitic stainless steel happens in mineral acids such as hydrochloric, sulfuric and nitric acids.[10,11] AISI 300 series austenitic steels are corroded by hydrochloric acid solutions.[11] Such attack is due to aqueous HCl dissociation yielding chloride ions, that attack the passive film formed on the steel.[11] In terms of steel chemistry, the addition of nickel typically increases the resistance to hydrochloric acid but makes the material susceptible to sulfide stress cracking.[12]

Localized Corrosion

Localized corrosion is a phenomenon associated with the formation of microscopic voids that develop on the steel surface due to high corrosion rates at specific zones.[10,11] This can result in pitting and intergranular corrosion, and potentially this can be associated with other types of localized corrosion (e.g., crevice corrosion and cracking). In particular, the formation of pits is a problem since their propagation has the potential to generate cracks and produce unexpected failures.[10] The onset of pitting corrosion in austenitic stainless steels is associated with attack by halide ions of the passive layer.[11] In order to overcome attack by halides ions, metallurgists have developed additional alloys within the AISI 300 series of austenitic stainless steels. These types of steel contain molybdenum as an alloying element that confers superior resistance to pitting corrosion.[6,10,11] There is a significant body of research relating to austenitic stainless steel corrosion mechanisms as well as studies relating to its mechanical properties.[6,10,11] However, these investigations relate to cold-rolled stainless steels. Conclusions from these studies cannot be casually extended to DMLS products since the microstructure and porosity of DMLS products are different. Consequently, the data reported herein is relevant since it provides foundational research on the effect of porosity and microstructure of a DMLS 316L stainless steel on its corrosion resistance. This work represents a first step to assess the applicability of using DMLS-type 316L stainless steel components in corrosive environments.

EXPERIMENTAL PROCEDURES

316L stainless steel DMLS specimens with and without cold work (CW) of 20% thickness reduction were tested and compared to an as-received commercial cold-rolled 316L SS. The chemical composition for the materials used in the present research is given in Table 1.

Table 1
Chemical composition (wt.%) of the 316L SS samples (as-rolled and DMLS), balance Fe

	Al	C	Cr	Cu	Mn	Mo	N	Nb	Ni	P	S	Si	Ti	W
Rolled	0.011	0.01	16.96	0.41	1.23	2.02	0.04	0.014	10.22	0.032	0.006	0.36	0.013	0.05
DMLS and DMLS CW	0.007	0.007	17.61	0.21	1.64	2.68	0.07	0.01	12.1	0.017	0.008	0.26	0.035	0.024

Some samples were solution annealed in an argon atmosphere to study the effect of scan tracks,[1–5] which are microstructural defects inherent to the DMLS process. The conditions are given in Table 2.

Table 2
Heat treatment for annealing

Heat Treatment	Conditions
Annealing in an argon atmosphere	1100 °C Soaking time: 45 min Argon quenched

Electrochemical Measurements

The anodic corrosion behavior of the specimens was studied by performing anodic potentiodynamic polarizations in a solution of 1N H_2SO_4 per ASTM G5[13] (scan rate of 0.1667 mV/s from -20 mV with respect to the open circuit potential up to 1.2 V vs Ag/AgCl reference electrode). Each condition was tested twice for repeatability. The experimental apparatus was a typical 3-electrode setup in a 2L glass cell, as shown in Figure 1. All the 316L SS samples were used as working electrodes. The specimens were cut to squares with a working area of 4 cm^2. The specimens were sequentially ground with 150, 400 and 600 grit silicon carbide paper, rinsed with isopropanol then sonicated for 5 minutes to remove any debris. A platinum-coated titanium mesh was used as the counter electrode. A saturated Ag/AgCl electrode was used as the reference electrode connected *via* a Luggin capillary. The electrolyte was a solution of 1N H_2SO_4. The test solution was prepared by mixing 55.6 mL of 98% H_2SO_4 with 1944.4 mL of deionized (DI) water.
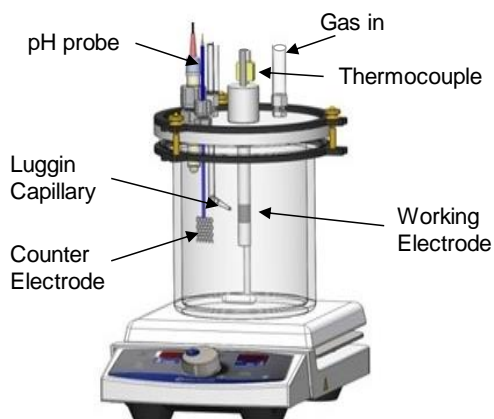

Figure 2: Three electrode glass cell setup to perform electrochemical measurements

Metallography

For metallographic characterization, similarly to the preparation described above, the specimens were sequentially ground with 150, 400 then 600 grit silicon carbide paper, rinsed with isopropanol and sonicated to remove any debris. After that, the specimens were successively polished with 9, 5, 1 and 0.25 µm diamond suspensions[14], rinsed with isopropanol and sonicated. Adler's reagent was utilized to reveal the austenitic grain structure. The chemical composition of the etchant is shown in Table 3.

Table 3
Chemical composition of the Adler's reagent

Reactant	Amount
Cupric ammonium chloride, dihydrate	9 g
Hydrochloric acid (concentrated)	150 mL
Ferric chloride, hydrated	45 g

Strain-Induced Martensite Determination

Possible formation of strain-induced martensite after cold working of DMLS specimens was assessed by X-ray diffraction (XRD). Data for the cold worked DMLS specimens were obtained with an X-ray diffractometer[†] (monochromatic CuKα radiation, λ = 0.15405 nm) at a scan rate of 2° min^{-1}. XRD was also performed on the DMLS as-received and rolled as-received specimens for comparative purposes.

Determination of Specimen Density

Since the 316L SS DMLS possesses inherent porosity, this would be expected to affect the density of the test specimens. Consequently, their densities were determined *via* the buoyancy effect technique as described in the ASTM B311 standard[15].

Pitting Corrosion Resistance

Pitting corrosion resistance was evaluated per ASTM G48[16]. A 6 wt.% $FeCl_3$ solution was utilized to simulate an aggressive environment to which each sample type (Rolled, Rolled with heat treatment, DMLS, DMLS with heat treatment, DMLS with cold work and DMLS with cold work and heat treatment) was exposed. Each group of samples consisted of four specimens, two polished with a 0.25 µm diamond suspension and two to a 600-grit finish; the finishes were applied after required heat treatments. The specimens were rinsed with isopropanol and sonicated for 5 minutes before immersion.

RESULTS AND DISCUSSION

Scan Tracks

Figure 3 shows representative arc-shaped microstructural defects known as scan tracks.[1–5] They are associated with the DMLS process. They are formed when the laser utilized to melt metal powder leaves a print during each individual melting point.
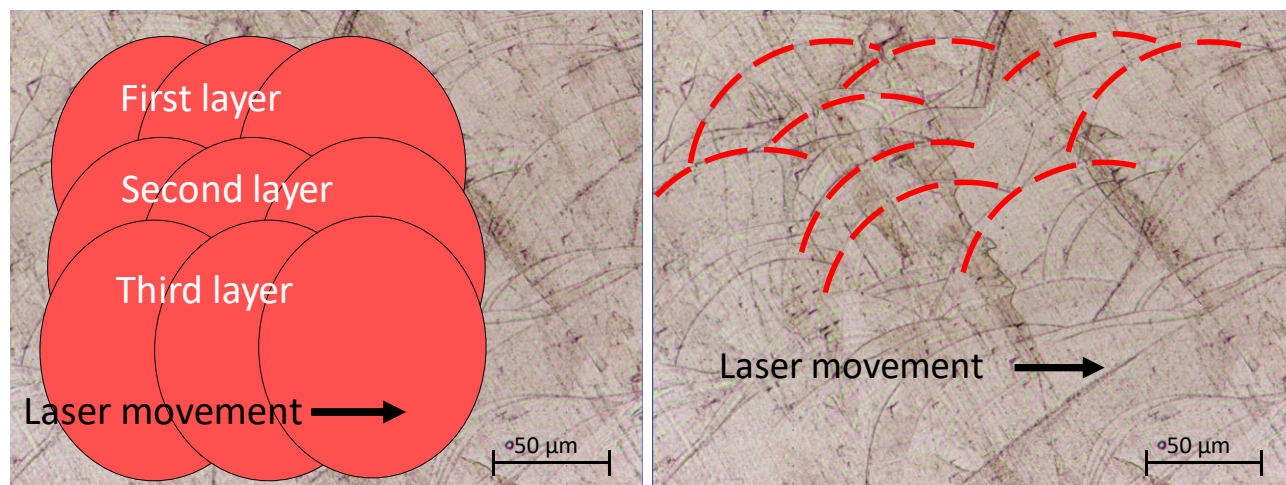

[†] Rigaku UltimaIV Difractometer

Figure 3: Arc-type microstructural defects known as scan tracks.[1–5] Layer-by-layer manufacturing process illustration (left) resulting in defects outlined in red dashed lines (right).

Heat Treatment and Metallography

The effect of heat treatment on the test materials was determined by metallographic characterization. Figure 4 shows the change in microstructure of the as-received materials compared with the heat treated specimens. In the case of the as-received cold-rolled material, the microstructure shows an increase in grain size. For the DMLS materials, the main effect of the heat treatment is the disappearance of the microstructural defects associated with the laser sintering (scan tracks). Figure 5 illustrates scan tracks present in the 316L SS DMLS and how they are eliminated after heat treatment.
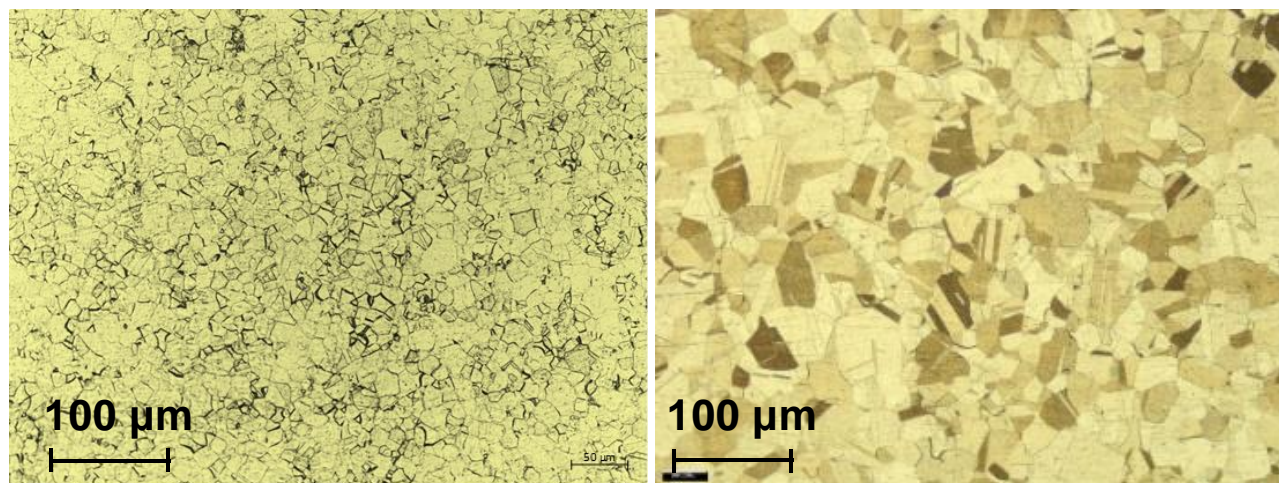
Figure 4: Heat treatment effect on a 316L SS specimen: as-received material (left), heat treated material (right).
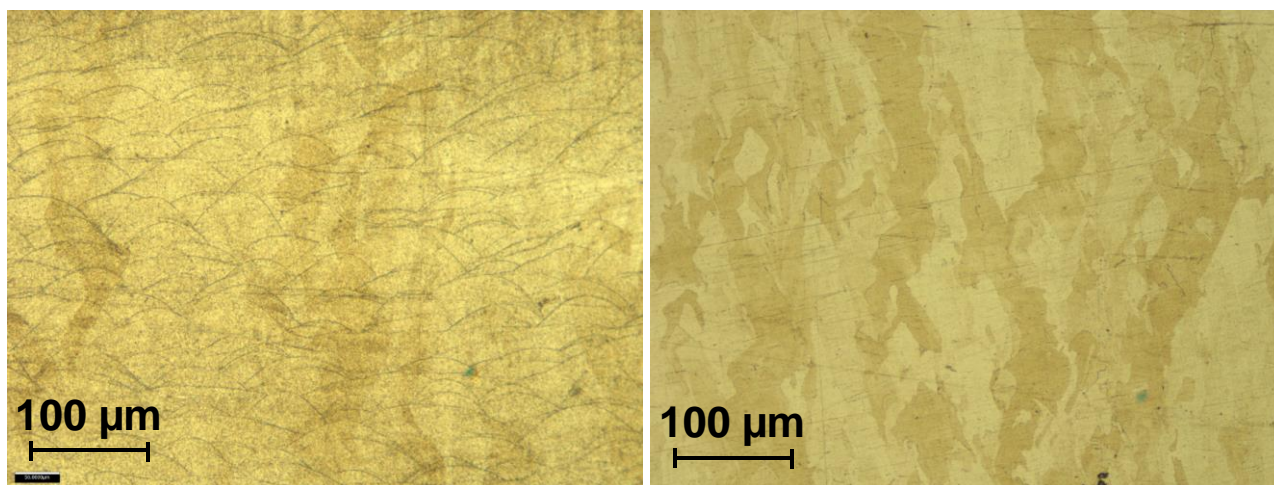
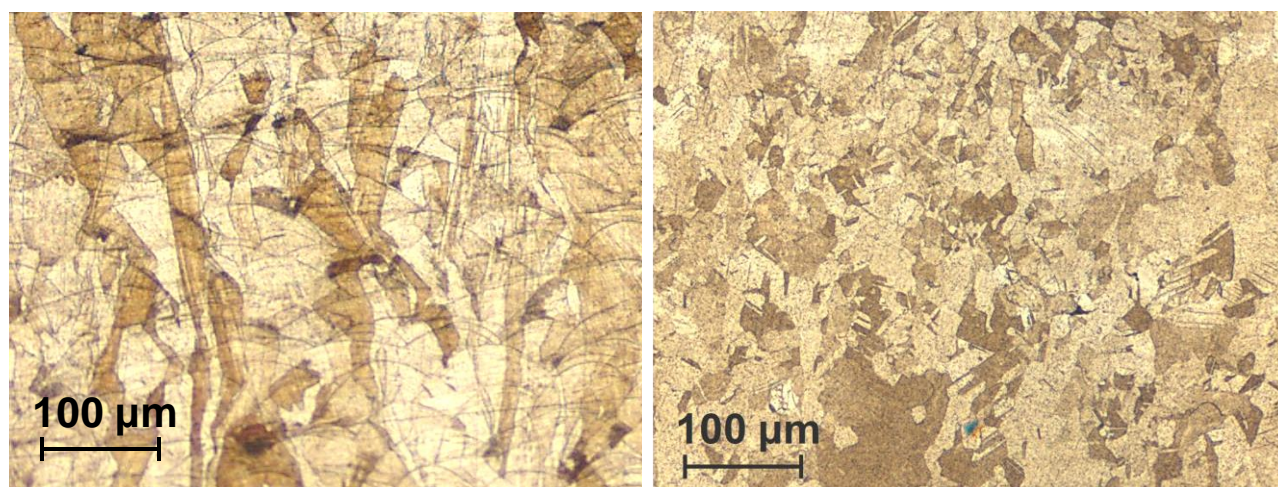**Figure 5: Heat treatment effect on a 316L SS DMLS specimen: as-received material (left), heat treated material (right). In the second microstructure the scan tracks disappeared as an effect of the heat treatment.**

Figure 6 shows a 316L SS DMLS after 20% thickness reduction by cold work and the effect of subsequent heat treatment. The micrograph on the left shows that after cold work the grains become deformed, in addition, change in scan track curvature is consistent with their elongation. In the right-hand-side picture, the heat treatment promoted a recrystallization of the grains, and the scan tracks were annihilated.

Figure 6: Heat treatment effect on a 316L SS DMLS Cold Work specimen: as-received material (left), heat treated material (right).

Strain-Induced Martensite

Since 20% thickness reduction cold work was applied on 316L SS DMLS specimens, the formation of strain-induced martensite (associated with α'-ferrite peaks) may have occurred[17]. Figure 7 shows the XRD patterns for this martensite assessment. In the case of the DMLS with no cold work, results indicated the presence of α'-ferrite as a minor phase given its peak intensity. When 20% thickness reduction cold work is applied, the intensity of the α'-ferrite peaks remains almost unchanged, which indicates that the formation of α'-ferrite due to cold work (associated with martensite) is negligible at this percentage of thickness reduction. In a similar fashion, α'-peaks in the as-rolled AR are of relatively low intensity with respect to the austenite peaks (γ).
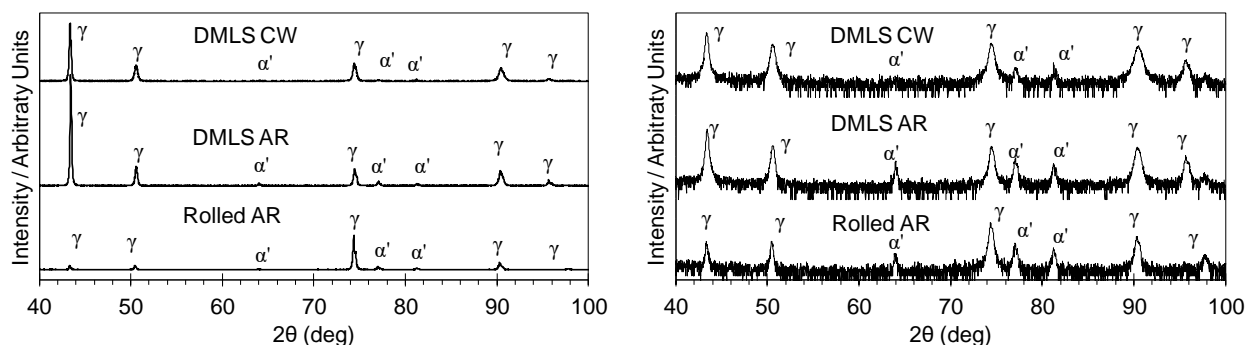
Figure 7: XRD patterns for three specimens: DMLS CW, DMLS AR and as-rolled AR. Austenite (γ) and α'-ferrite are indicated by their corresponding peaks. Intensity in linear scale (left) and in logarithm scale (right).

Electrochemical Measurements

Figure 8 shows anodic potentiodynamic polarization curves for the rolled and DMLS 316L stainless steel specimens for various conditions; namely as-received (A), heat treated (B) and cold worked (C). In the first plot (A), the anodic behavior of the DMLS specimen is compared to the anodic behavior of the rolled material. Despite the passivation zone originating in the same potential region for both as-received specimens, the passive current density of the DMLS 316L stainless steel is almost 8 times higher than the rolled material. This result suggests that even though the DMLS 316L stainless steel displays a similar passive behavior compared to the rolled material, the corrosion resistance of its passive layer is much weaker. In the second plot (B), the effect of the heat treatment is shown. The passive current density of the rolled 316L stainless steel specimen decreased, while it did not exhibit a significant change for the DMLS material. This suggests that the annihilation of scan tracks may not have a significant effect on the corrosion properties of the passive film. Finally, the third graph (C) of Figure 8 shows that the cold work has a detrimental effect on the passivation curve of the DMLS 316L stainless steel since the passive current density increased by *ca.* a factor of 10. This condition suggests that cold work has a detrimental effect on the properties of the passive film as the cold worked 316L SS DMLS specimen corrodes at a higher rate than the specimen without cold work. The graph also shows that heat treatment restores the corrosion resistance properties of the 316L SS DMLS material as the heat treated specimen exhibits a significantly lower passive current density than its "as-received" and "cold worked" counterparts.
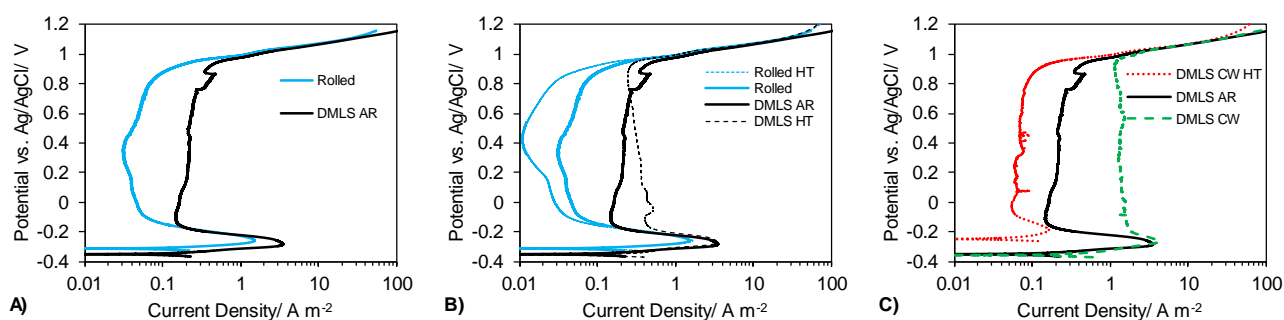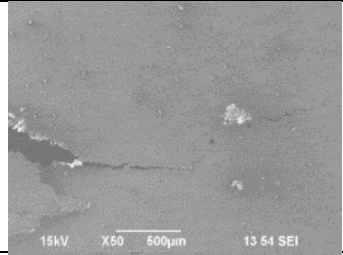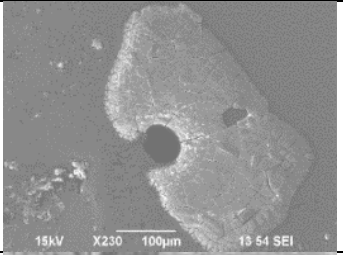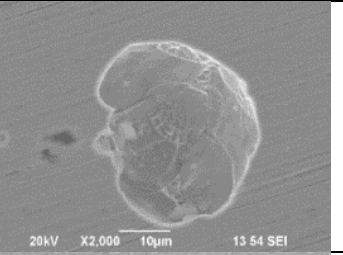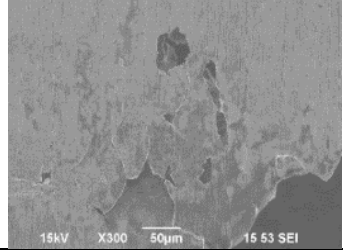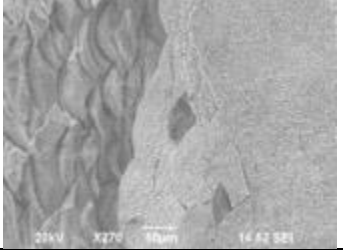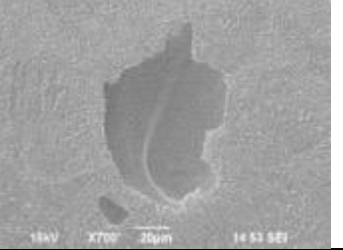

Figure 8: Anodic behavior of the 316L SS specimens. A) Rolled as received (AR) and DMLS AR. B) Rolled AR and heat treated (HT), DMLS AR and DMLS HT. C) DMLS AR, DMLS cold worked (CW) and DMLS CW HT.

Corrosion Initiation Mechanisms (Ferric Chloride Corrosion Test)

In order to obtain a qualitative analysis of the corrosion initiation mechanism for the 316L SS DMLS, a ferric chloride corrosion test was performed in 6 wt.% aqueous $FeCl_3$ at 55°C with a specimen exposure

duration of 2 days. Microscopic characterization of the 316L stainless steel specimens after the corrosion test provided key information about the mechanisms of corrosion and the detected pitting morphology. Table 4 shows the surfaces of the as-received rolled and DMLS 316L stainless steel specimens after the corrosion test. The pit appearance and pit morphology are also shown. The images show that there is not a well-defined pattern for corrosion in the rolled material, whereas the corrosion seems to be preferentially initiated on microstructural defects (scan tracks) in the DMLS specimens. The pit morphology in the rolled sample indicates a semi-spherical shape, whilst the pits in the DMLS 316L stainless steel specimens shows an irregular pattern associated with scan tracks of the material.

Table 4
General corrosion and pit morphology for as-received specimens after FeCl$_3$ corrosion tests

	General Corrosion	Pitting Appearance	Pit Morphology
Rolled As-Received			
DMLS As-Received			

Optical microscopy was utilized to investigate the preferential corrosion initiation in the DMLS 316L stainless steel specimens. Figure 9 shows that the corrosion is initiated at the scan tracks. Figure 10 also indicates that the growth of the corroded features follows the scan track patterning.
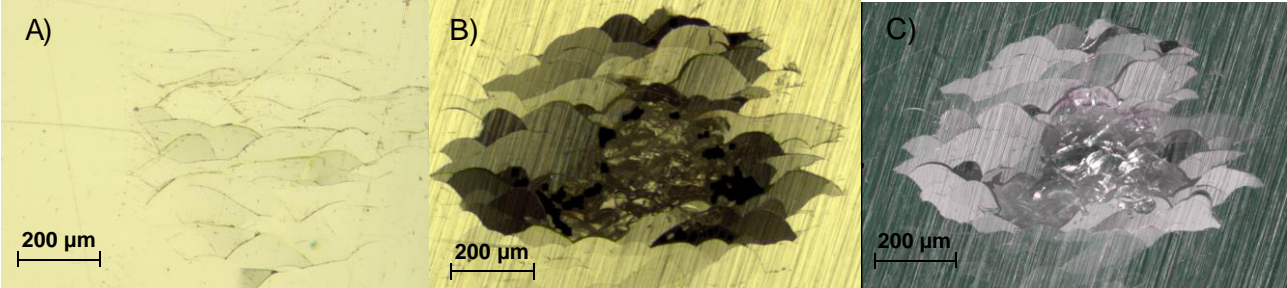

Figure 9: General corrosion initiation of the DMLS 316L stainless steel as-received material characterized by optical microscopy: A) Zone with corrosion initiation, B) Zone with damage from corrosion, C) same zone as B) with a polarized lens filter.
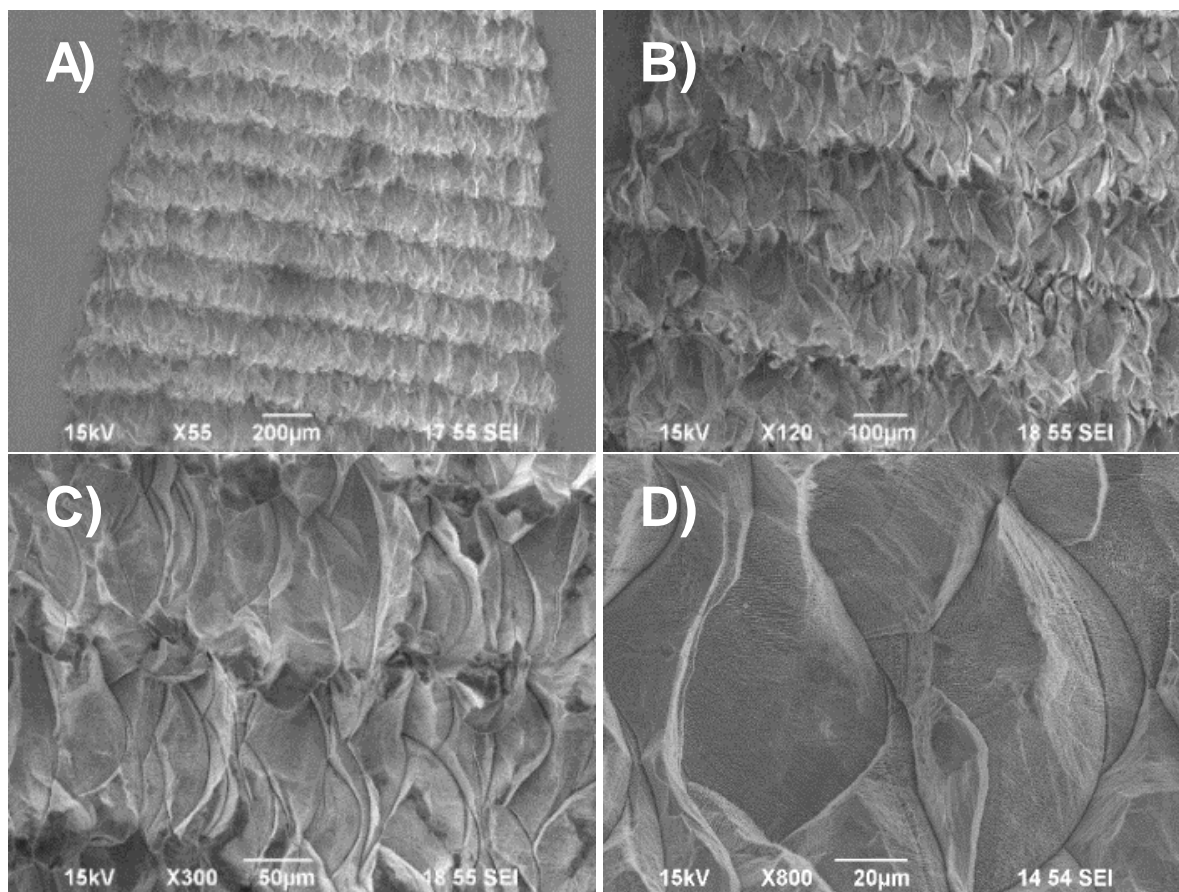
Figure 10: General corrosion of the DMLS 316L stainless steel material: A) general appearance; B), C) and D) zooms in on the affected zones

The morphology of the corroded surface of the DMLS 316L stainless steel specimens after heat treatment was characterized by SEM, as shown in Figure 11. The images show that the corrosion did not follow any obvious pattern associated with scan tracks. This also suggests that the heat treatment diminished the susceptibility of DMLS material to suffer from preferential corrosion on scan tracks, as compared to the as-received material (as shown in Figure 10). Finally, the pit morphology of the heat treated 316L SS DMLS specimen seems to follow a spherical pattern, confirming that the corrosion is not preferentially initiated on scan tracks.
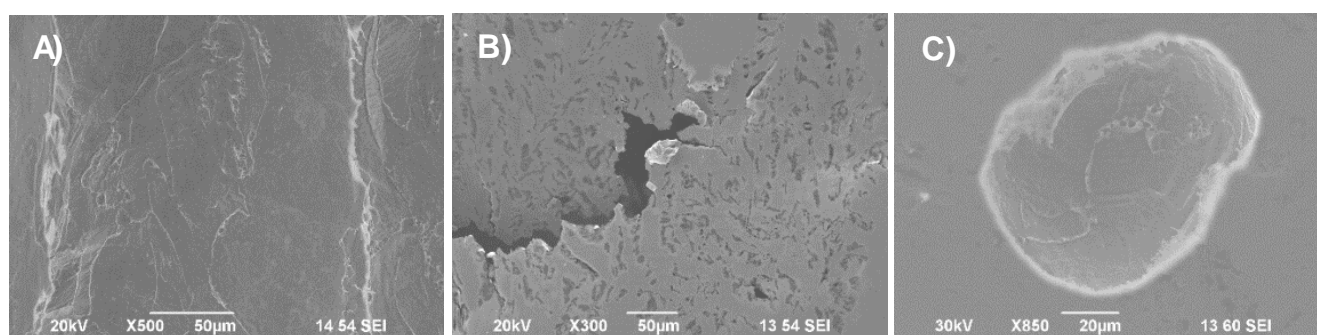
Figure 11: General corrosion of the DMLS 316L stainless steel specimens following heat treatment: A) general appearance, B) corrosion initiation, C) pit morphology

Possible explanations for preferential corrosion through the scan tracks are the formation of crevices due to void fraction or porosity inherent from the DMLS manufacturing process or due to chemical segregation of alloying elements at the edge of the scan tracks. Both possibilities were explored as follows.

Porosity

Figure 12 shows the microstructure of a DMLS AR specimen before the corrosion test. The specimen was successively ground and polished up to 0.25 µm and etched (Adler's reagent). Note the spaces between the scan tracks; such voids are better observed with a 3D profilometry plot, shown in Figure 13.
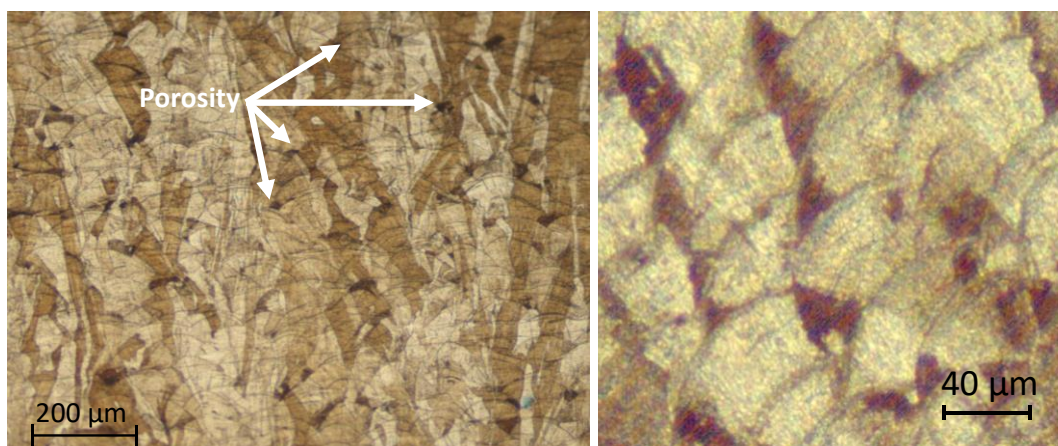
Figure 12: Porosity in the DMLS specimens: low magnification (left), high magnification (right)
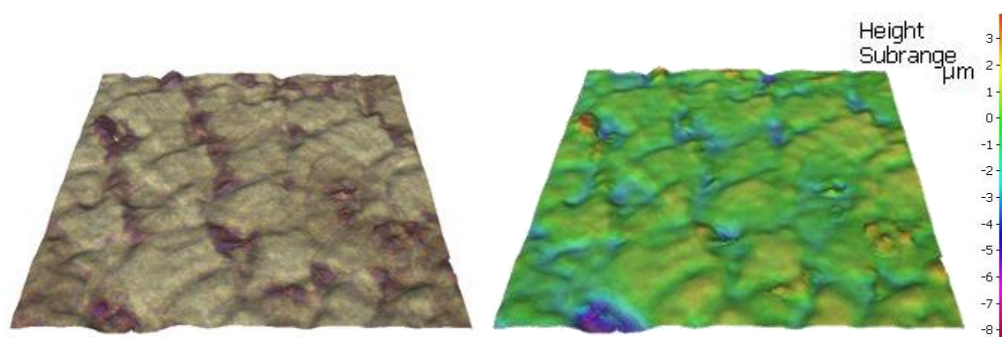
Figure 13: 3D plot of the scan tracks at high magnification (see Figure 12 right).

Chemical Segregation of Alloying Elements

Microsegregation of alloying elements, in particular molybdenum, has been reported as a problem relating to the corrosion resistance of superaustenitic stainless steel welds[18–20]. Since the DMLS manufacturing process bears a certain similarity to welding (rapid melting and solidification of metal used to coalesce material), and the fact that the SEM shown in Figure 14 shows the presence of dark and light areas, the presence of microsegregation of elements can be postulated to occur within the interdendritic structure.[18] Therefore, microsegregation of elements can be hypothesized to occur within the dendritic structure of the DMLS specimens, causing preferential localized corrosion in DMLS specimens. In order to test this hypothesis, energy-dispersive X-ray spectroscopy (EDS) was used to characterize the void surfaces to determine their local chemical composition adjacent to the perimeter (boundaries) of the scan tracks. The EDS data shown in Figure 14 shows that there is no significant compositional difference between the edge of the scan track and the adjacent zone. Consequently, there is no conclusive evidence of microsegregation of any element within the scan track boundary. However, Figure 15 shows a 316L SS DMLS etched sample. EDS analysis was performed on the dark and light phases of a zone contiguous

to a scan track. These analyses showed that some elements are present in different concentration within the phases. Thereby, the microsegregation of elements might play a significant role in the preferential corrosion of the DMLS specimens.
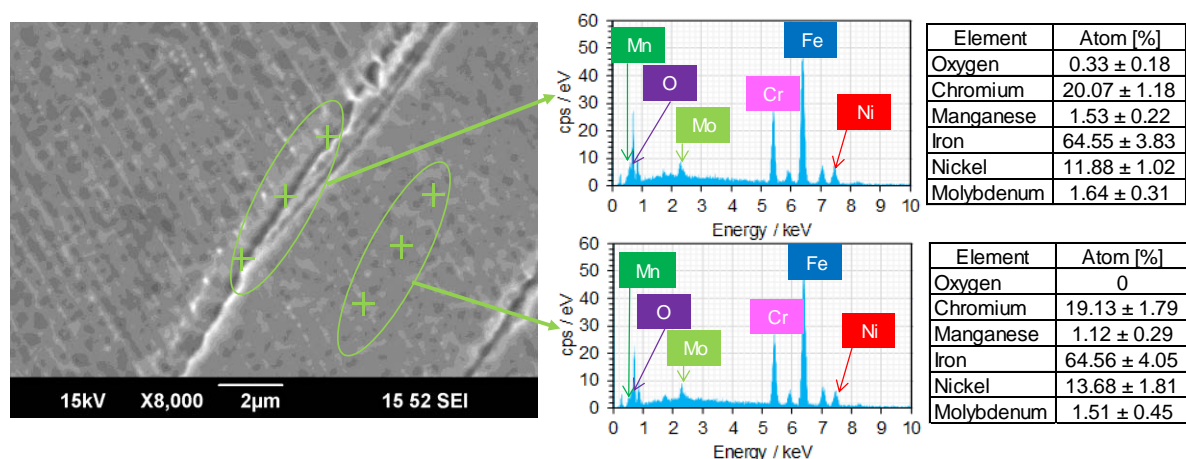

Element	Atom [%]
Oxygen	0.33 ± 0.18
Chromium	20.07 ± 1.18
Manganese	1.53 ± 0.22
Iron	64.55 ± 3.83
Nickel	11.88 ± 1.02
Molybdenum	1.64 ± 0.31

Element	Atom [%]
Oxygen	0
Chromium	19.13 ± 1.79
Manganese	1.12 ± 0.29
Iron	64.56 ± 4.05
Nickel	13.68 ± 1.81
Molybdenum	1.51 ± 0.45

Figure 14: EDS analyses of a scan track and its contiguous adjacent area[‡].

Element	Atom [%]
Oxygen	1.64 ± 0.84
Chromium	28.96 ± 2.86
Manganese	5.83 ± 0.86
Iron	50.77 ± 5.13
Nickel	1.57 ± 0.52
Molybdenum	0.71 ± 0.43

Element	Atom [%]
Oxygen	1.43 ± 0.21
Chromium	22.38 ± 1.38
Manganese	4.98 ± 0.47
Iron	44.40 ± 2.78
Nickel	3.96 ± 0.56
Molybdenum	2.78 ± 0.81
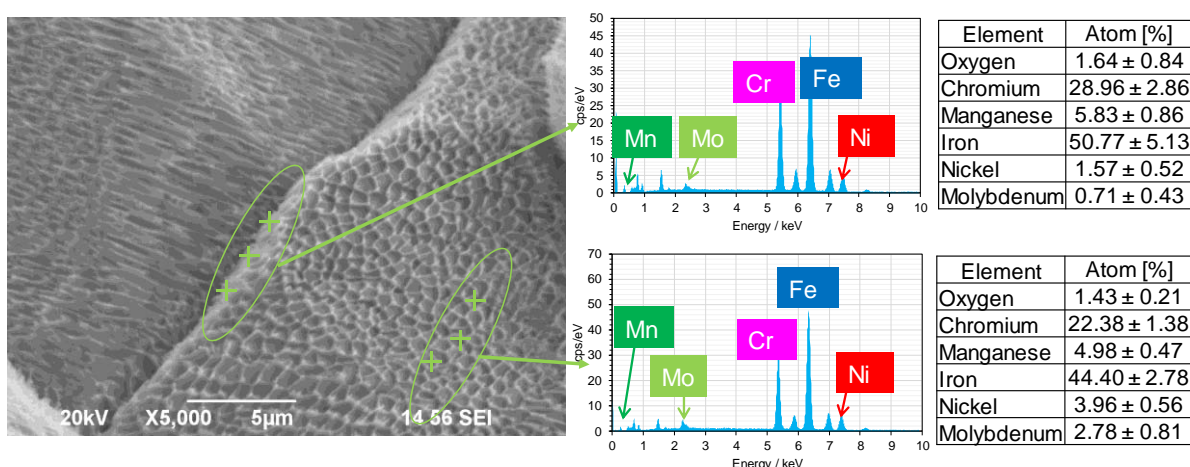
Figure 15: EDS analyses of dark and light phases adjacent to a scan track boundary

Pit Analysis

Since the pitting behavior seems to be influenced by the inherent microstructural defects in the 316L SS DMLS specimen, at least in the absence of heat treatment, the morphology of the pits was characterized by SEM/EDS and profilometry. Table 5 shows the different morphologies, chemistries and related profilometry data of the pits generated in the ferric chloride corrosion test. For all the materials the chromium content did not vary significantly with respect to the chemical composition presented in Table 5 (ranging from 23 to 27%). However, other elements were significantly affected. For instance, in the rolled AR, nickel concentration decreased from 12 to 1.75 wt.% and the molybdenum concentration decreased by a factor of 2. Other specimens suffered alloy depletion in a similar fashion. Those changes in local chemistry can be attributed to the corrosion product formed inside the pit due to the high observed oxide content.

[‡] EDS data acquired by Mr. Michael Spencer, Department of Mechanical Engineering, Ohio University.

Table 5
SEM, and EDS and Profilometry of Selected Pits after FeCl₃ Corrosion Tests

	SEM	EDS Spectra	EDS %	Profilometry
Rolled AR			Element / Atom [%]: Oxygen 2.76, Chlorine 5.03, Chromium 25.84, Manganese 2.51, Iron 60.83, Nickel 1.75, Molybdenum 1.28	Depth: 90µm
DMLS AR			Element / Atom [%]: Oxygen 2.71, Chlorine 0.34, Chromium 26.94, Manganese 1.67, Iron 56.93, Nickel 8.72, Molybdenum 2.69	Depth: 50µm
DMLS CW			Element / Atom [%]: Oxygen 0.02, Chlorine 0.06, Chromium 23.9, Manganese 1.94, Iron 62.11, Nickel 11.13, Molybdenum 0.84	Depth: 50µm
Rolled HT			Element / Atom [%]: Oxygen 1.45, Chlorine 0, Chromium 22.68, Manganese 1.57, Iron 66.85, Nickel 6.42, Molybdenum 1.04	Depth: 200µm
DMLS HT			Element / Atom [%]: Oxygen 4.12, Chlorine 0.28, Chromium 23.96, Manganese 2.27, Iron 57.25, Nickel 9.39, Molybdenum 2.73	Depth: 50µm
DMLS CW HT			Element / Atom [%]: Oxygen 5.44, Chlorine 0.17, Chromium 23.4, Manganese 1.81, Iron 56.95, Nickel 9.68, Molybdenum 2.54	Depth: 50µm

Statistical Analysis of Pit Distribution

The Weibull distribution has been utilized to model the distribution of pits in austenitic stainless steels[10,21]. The purpose of using the Weibull distribution in this research is to determine if there is a significant difference in the pit depth and pit diameter distribution among the different specimens. The cumulative density function (cdf) for the Weibull distribution is given by[22]:

$$F(t) = 1 - \exp\left(-\left(\frac{t}{\eta}\right)^{\beta}\right)$$

(1)

Where: $F(t)$ is the frequency as a function of a parameter t (the measurement for which a probability of appearance is calculated. In this research, the pit diameter or the pit depth), η is the scale parameter (a measure of the dispersion of the data) and β is the shape parameter (how similar the distribution is in relation to a normal, "bell-shaped" distribution).

To determine if the data can be represented by a Weibull distribution, the parameters η and β are estimated through linearizing Equation (1)[22]:

$$\ln\left(-\ln\left|1 - F(t)\right|\right) = \beta \ln(t) - \beta \ln(\eta)$$

(2)

Equation (2) is analogous to a linear equation, where β is the slope and the parameter $-\beta \ln(\eta)$ is the intersection of the line. By using the least square method, the validity of the fit is determined. Finally, after obtaining the parameters for the Weibull distribution, the probability density function for each condition was determined with the following equation, which is known as the 2-Parameter Weibull distribution[22]:

$$F(t) = \frac{\beta}{\eta}\left(\frac{t}{\eta}\right)^{\beta-1} \exp\left(-\left(\frac{t}{\eta}\right)^{\beta}\right)$$

(3)

With the mean ($\bar{T}$) given by:

$$\bar{T} = \eta \cdot \Gamma\left(\frac{1}{\beta} + 1\right)$$

(4)

And the standard deviation:

$$\sigma = \eta \sqrt{\Gamma\left(\frac{2}{\beta} + 1\right) - \Gamma\left(\frac{1}{\beta} + 1\right)^2}$$

(5)

Where Γ is the gamma function defined as $\Gamma(x) = \int_0^{\infty} e^{-x} x^{n-1} dx$.

The diameter and the depth of the pits were measured and organized as a function of their frequency. The histograms and their respective Weibull distribution for pit depth and pit diameter are presented in Table 6 and Table 7.

Regarding the as-received specimens, the Weibull distribution mean for the pit depth in rolled specimen is close to 13 μm, while the DMLS specimen showed a mean of 22 μm. On the other hand, the DMLS cold worked specimen (DMLS CW) exhibited a slightly higher mean pit depth (*ca.* 31 μm). The average pit depth of the DMLS CW is notoriously affected by the heat treatment since the average pit depth increased by a factor of 5 to 6. In the case of the rolled material, the average depth increased from 13 to *ca.* 73 μm. For the DMLS specimen, the average pitting depth increased from 22 to *ca.* 70 μm.

Similarly, the pit diameter distribution was also affected by the heat treatment. The average pit diameter for the rolled material was *ca.* 40 μm. After the heat treatment, the average increased to *ca.* 143 μm. The

same behavior was observed for the DMLS specimens. The average pit diameter increased from 32 to 105 µm. Finally, the average pit diameter for the DMLS CW specimen was also affected as the average increased from 26 to 203 µm.

Table 6
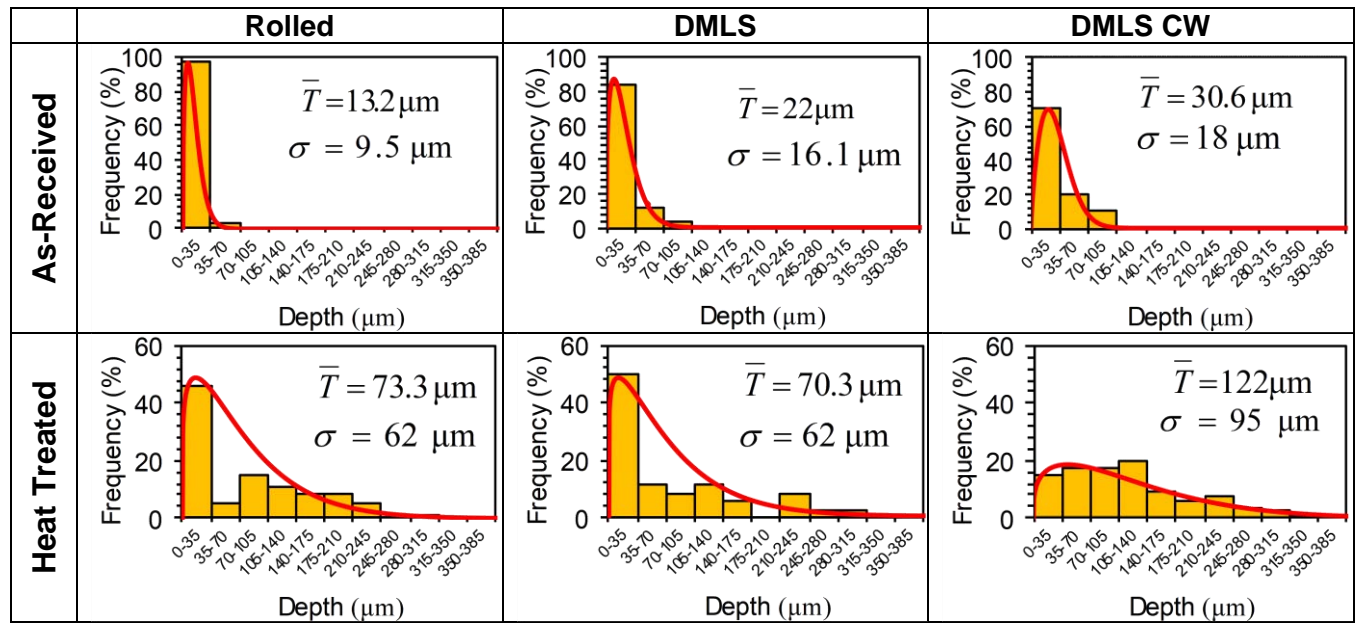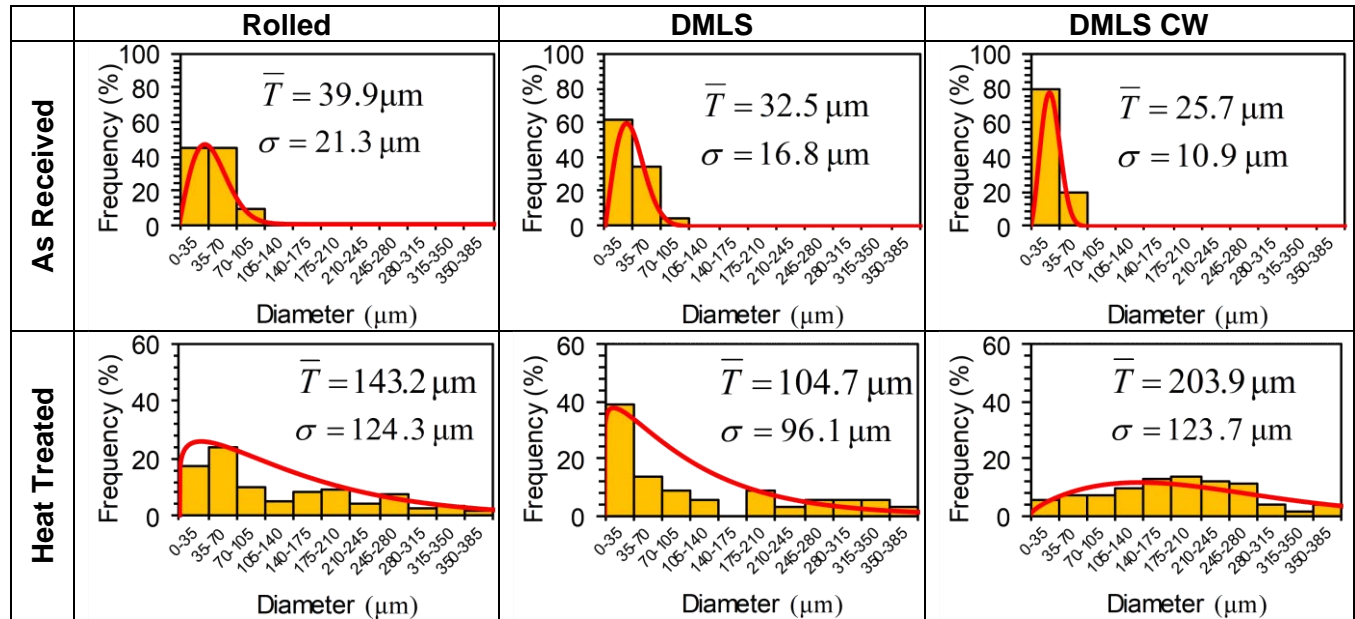**Weibull distribution for pit depth in the 316L stainless steel specimens**

Table 7
Weibull distribution for pit diameter in the 316L stainless steel specimens

General Corrosion Resistance

It must be stated that the corrosion rates were calculated for comparative purposes only. Since the ferric chloride corrosion solution is very aggressive and unrealistic, the information obtained from such a test must be interpreted with caution. Having made this clarification statement, to measure the corrosion resistance of the specimens, the general corrosion rate (*CR*) was obtained using the general formula:

$$CR = \frac{\Delta m}{A \rho t} \tag{6}$$

Where: Δm is the weight loss during the corrosion test, A is the exposed area of the sample, ρ is the density of the material, and t is the test duration.

The comparative corrosion rates for each specimen tested are given in Figure 16.
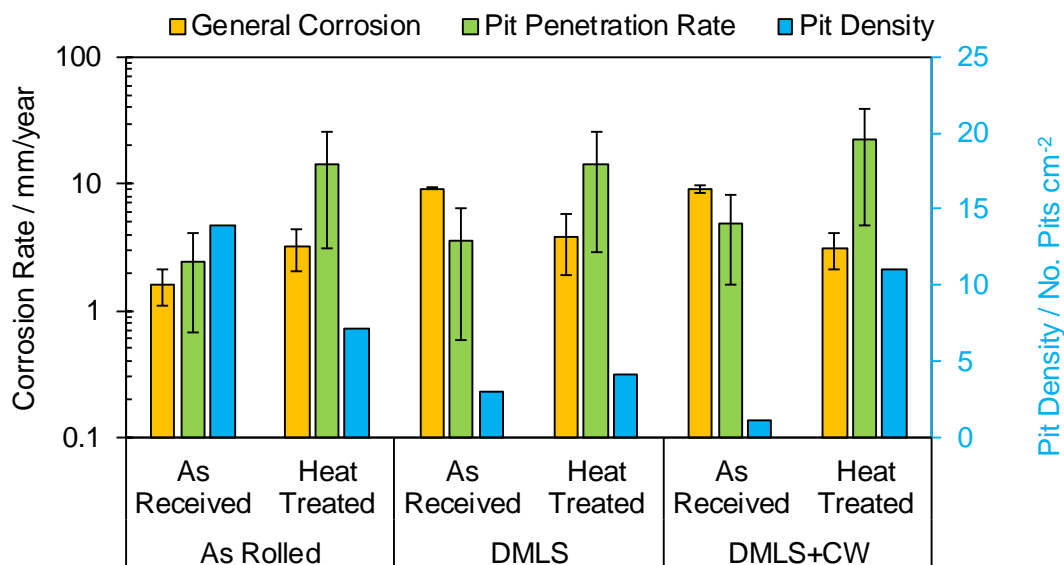

Figure 16: Corrosion rates for 316L stainless steel specimens.

Figure 16 shows the general corrosion rate, the pit penetration rate and the pit density for each of the different 316L stainless steel specimens heretofore discussed. The rolled as-received specimen exhibited a corrosion rate of *ca.* 2 mm/year. In comparison, the DMLS as-received specimen corroded five times faster. Such high corrosion rates were also observed in the 316L DMLS specimens with cold work without heat treatment. The high corrosion rate can then be explained by Figure 10, which shows that the corrosion propagated through the scan tracks. This led to detachment of a significant amount of material that subsequently increased the calculated corrosion rates. In general, the heat treatment reduced the corrosion rate in DMLS specimens. However, the general corrosion resistance of DMLS specimens is significantly lower than that of the rolled as-received 316L stainless steel specimens. The pit penetration rate corresponds to the average pit depth obtained from the Weibull distribution divided by the test time (2 days). In terms of pit penetration rate, the heat treatment had a different effect on each sample. Regarding the as-received cold-rolled 316L SS, the heat treatment increased the pit penetration rate and, at the same time, decreased the pit density. One possible explanation for this is that small precipitates were dissolved by the heat treatment, leading to a diminution in observed post-test pit density; this effect is being studied in on-going research. Concerning the DMLS samples, the as-received DMLS and cold worked DMLS specimens had lower pit density (number of pits *per* unit of area). In the case of the cold worked DMLS specimens, the heat treatment had a negative effect since the pit density increased.

Finally, the bulk densities of the specimens were measured before and after the corrosion test to determine if the inherent porosity of the DMLS specimens can be related to the corrosion process. Figure 17 shows that the initial bulk density of the DMLS specimens (before corrosion testing) is lower than the rolled material. Such a lower density can be associated with porosity within the DMLS specimens. The lower the bulk density with respect to the rolled material is, the higher the intrinsic porosity will be. It was observed that specimens with the lowest bulk densities showed a higher general corrosion rate (as seen in Figure 16). Such a trend can be explained by assuming that the porosity is related to the active area of the samples. In this way, DMLS specimens contain more surface area in contact with the aggressive environment produced by the 6 wt.% $FeCl_3$, leading to a higher corrosion rate in comparison to the rolled samples with lower porosity.
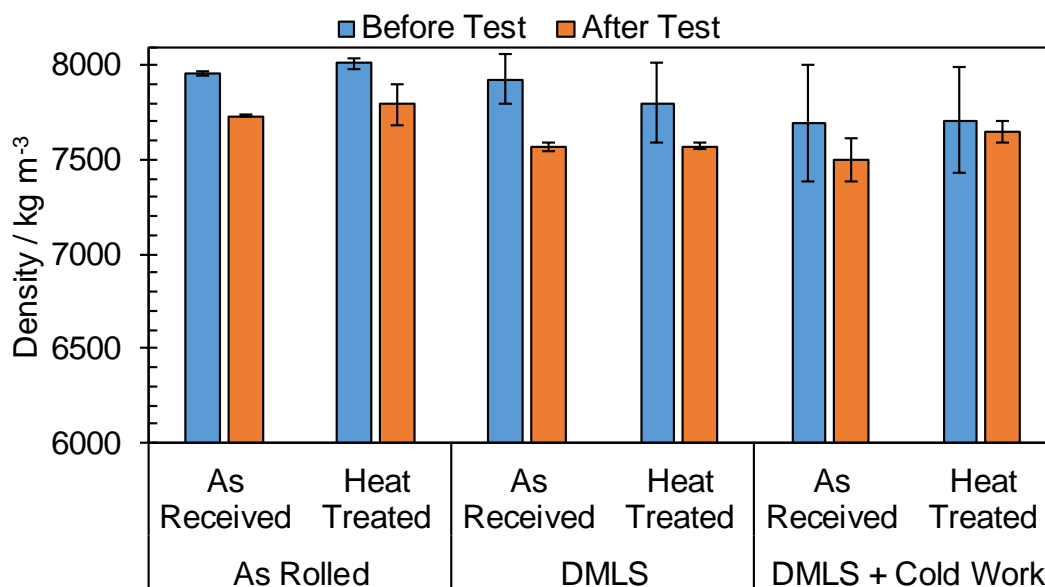

Figure 17: Density of the 316L stainless steel rolled and DMLS specimens before and after corrosion tests.

CONCLUSIONS

- 316L stainless steel specimens made by direct metal laser sintering (DMLS) corroded preferentially through the microstructural defects inherent to the manufacturing process (scan tracks).
- The preferential corrosion can be attributed to voids and porosity on the surface due to the sintering process as well as chemical segregation within the boundaries of the scan tracks.
- Heat treatment reduced the presence of microstructural defects (scan tracks) in DMLS specimens. Such a condition changed the corrosion damage patterns and the morphology of pits formed.

ACKNOWLEDGMENTS

REFERENCES

1   I. Gibson, D. Rosen, and B. Stucker, *Additive Manufacturing Technologies*, 1st ed. (New York, NY: Springer, 2010), pp. 1-42

2   J. P. Kruth, P. Mercelis, J. Van, V. L. Froyen, M. Rombouts, J. Van Vaerenbergh, and L. Froyen, "Binding mechanisms in selective laser sintering and selective laser melting," *Rapid Prototyp. J.*, 11, 5, (2005): pp. 314-326.

3   S. S. Panda, V. Singh, A. Upadhyaya, and D. Agrawal, "Sintering response of austenitic (316L) and ferritic (434L) stainless steel consolidated in conventional and microwave furnaces," *Scr. Mater.*, 54, 12, (2006): pp. 2179-2183.

4   A. Simchi, F. Petzoldt, and H. Pohl, "On the development of direct metal laser sintering for rapid tooling," *J. Mater. Process. Technol.*, 141, 3, (2003): pp. 319-328.

5   R. M. Molak, K. Paradowski, T. Brynk, L. Ciupinski, Z. Pakiela, and K. J. Kurzydlowski, "Measurement of mechanical properties in a 316L stainless steel welded joint," *Int. J. Press. Vessel. Pip.*, 86, 1, (2009): pp. 43-47.

6   M.McGuire, *Stainless Steels For Design Engineers*, 1st ed. (Materials Park, OH: ASM International, 2008), pp. 69-90.

7   L.-Å. Norström, "The influence of nitrogen and grain size on yield strength in Type AISI 316L austenitic stainless steel," *Met. Sci.*, 11, 6, (1977): pp. 208-212.

8   S. A. Maloy, M. R. James, G. Willcutt, W. F. Sommer, M. Sokolov, L. L. Snead, M. L. Hamilton, and F. Garner, "The mechanical properties of 316L / 304L stainless steels , Alloy 718 and Mod 9Cr ± 1Mo after irradiation in a spallation environment," *J. Nucl. Mater.*, 296, (2001): pp. 119-128.

9   K. Sugimoto and Y. Sawada, "The Role of Molybdenum Additions to Austenitic Stainless Steels in the Inhibitoin of Pitting in Acid Chloride Solutions," *Corros. Sci.*, 17, (1977): pp. 425-445.

10   R. R. Winston and H. H. Uhlig, *Uhlig's Corrosion Handbook*, 3rd ed. (Pennington, NJ: Wiley & Sons, 2011), pp.657-693.

11   H. Khatak and B. Raj, *Corrosion of austenitic stainless steels: mechanism, mitigation and monitoring*, 1st ed. (Pangbourne, UK: Alpha Science International Ltd., 2002).

12   M. Kappes, M. Iannuzzi, R. B. Rebak, and R. M. Carranza, "Sulfide stress cracking of nickel-containing low-alloy steels," *Corros. Rev.*, 32, 3-4, (2014): pp. 101-128.

13   G5 (latest revision), "Standard Reference Test Method for Making Potentiodynamic Anodic Polarization Measurements" (West Conshohocken, PA: ASTM International).

14   B. L. Bramfitt and a. O. Benscoter, *Metallographer's Guide Practise and Procedures for Iron and Steels*, 1st ed. (Materials Park, OH: ASM International, 2002).

15   ASTM B311 (latest revision), "Standard Test Method for Density of Powder Metallurgy (PM) Materials Containing Less Than Two Percent Porosity" (West Conshohocken, PA: ASTM International).

16   ASTM G48 (latest revision), "Standard Test Methods for Pitting and Crevice Corrosion Resistance of Stainless Steels and Related Alloys by Use of Ferric Chloride Solution" (West Conshohocken, PA: ASTM International).

17   H. Abreu, S. Carvalho, and P. Lima, "Deformation Induced Martensite in an AISI 301LN Stainless Steel: Characterization and Influence on Pitting Corrosion Resistance," *Materials Research*, 10,4. (2007): pp. 359-366.

18   S. W. Banovic and J. N. DuPont, "Dilution and Microsegregation in Dissimilar Metal Welds Between Super Austenitic Stainless Steel and Nickel Base Alloys," *Sci. Technol. Weld. Join.*, 7. (2002): pp. 374-383.

19   T. D. Anderson, M. J. Perricone, J. N. DuPont, and A. R. Marder, "The Influence of Molybdenum on Stainless Steel Weld Microstructures," *Weld. J.*, 86. (2007): pp. 281-292.

20   M. Quian and J. N. DuPont, "Microsegregation-related Pitting Corrosion Characteristics of AL-6XN Superaustenitic Stainless Steel Laser Welds," *Corros. Sci.*, 52. (2010): pp. 3548-3553.

21   P. M. Aziz, "Application of the Statistical Theory of Extreme Values To the Analysis of Maximum Pit Depth Data for Aluminum," *Corrosion*, 12, 10. (1956): pp. 35-46.

22   J. I. McCool, *Using the Weibull distribution: reliability, modeling and inference*, 1st ed., (New York, NY: John Wiley & Sons, 2012), pp. 64-103.